Extreme Wave Generation, Breaking and Impact Simulations using Wave Packets in REEF3D

Hans Bihs[1], Arun Kamath*[1], Mayilvahanan Alagan Chella[1], and Øivind A. Arntsen[1]

[1]Department of Civil and Environmental Engineering, Norwegian University of Science and Technology (NTNU), 7491 Trondheim, Norway

Journal of Offshore Mechanics and Arctic Engineering, 2019, **141** (4), pp. 041802-1–041802-7.
DOI: http://dx.doi.org/10.1115/1.4042178

Abstract

On several occasions freak waves have been observed in the past, some causing severe damage. In order to model such extreme wave conditions, one possibility is to use focused waves of first or second order based on irregular sea state wave spectra. The wave phase is chosen such that the waves focus at a predetermined location and time, but the individual wave components become steep and start breaking before the focus location for large amplitudes. In this study, transient wave packets are used for extreme wave generation. Extreme waves are generated that are higher and only break at the concentration point using the transient wave packets method implemented in the open-source CFD model REEF3D. Model validation is performed by comparison to experimental results. The generation of wave packets with an 8.3 times shorter focus distance is investigated and the wave is replicated in a shorter domain with a 9% higher crest. The method is further used to generate a steepness induced-breaking wave and calculation of extreme wave forces on an offshore structure is demonstrated.

Keywords: Wave packets; Extreme waves; Breaking waves CFD; Computational Fluid Dynamics; REEF3D

1 Introduction

At sea, the occurrence of extreme waves is of stochastic nature. Experimental investigations to determine response of offshore structures involve irregular wave generation over three hours

*Corresponding author, arun.kamath@ntnu.no
Postprint, published in Journal of Offshore Mechanics and Arctic Engineering, doi:http://dx.doi.org/10.1115/1.4042178

to replicate the full spectrum and attain stationary conditions under the testing programme. Time domain numerical simulations for the same conditions is also computationally expensive. While the structural response under operational conditions can be determined through frequency domain numerical methods time-domain methods are recommended for extreme wave interaction where both physical and statistical properties of the waves in a highly non-linear phenomenon are important. Several methods in the time-domain for determining the design extreme wave for offshore structures have been developed over time such as a large regular wave Soares (1993), random irregular waves Wang (2001), identification of critical wave episodes Torhaug (1996) and the most likely extreme response (MLER) Tromans et al. (1991) Hansen and Nielsen (1995) where an irregular wave train is conditioned to produce a linear extreme wave with a prescribed response profile at a prescribed time. The MLER method can be considered a generalisation of the critical wave episodes method Pastoor et al. (2003).

The New Wave formula Tromans et al. (1991) is one of the MLER methods is based on the linear wave theory and a wave spectrum such as the JONSWAP or PM spectrum can be used for wave generation of the wave components. Due to its dependence on the linear wave theory, it requires the use of stretching methods such as Wheeler (1969) to account for the kinematics above the mean water level, which become important for extreme waves. There are some methods that do not require application of stretching to define large amplitude waves. One such approach to generating an extreme wave event, is the Gaussian wave packets Clauss and Bergmann (1986) Phillips et al. (1993) where the wave components in a finite length wave train superimpose at a prescribed point. With improved computational methods, the restriction on the wave amplitudes to be Gaussian distributed to allow for analytical solutions was no longer necessary. A transient wave technique where the shape and width of the wave spectrum is selected individually was proposed by Clauss and Kuehnlein Clauss and Kuehnlein (1997). An upstream transformation is carried out from the concentration point of the extreme wave using the Fourier transform to obtain the original wave train that resulted in the focused extreme wave. This method provides a better representation of the physical reality with a continuously changing propagating wave envelope in comparison to an artificial standard wave packet Rozario et al. (1993).

In terms of time domain simulations of extreme wave events, several studies using focused waves are presented in current literature. Wave interaction with a vertical cylinder with for non-breaking extreme waves using OpenFOAM Chen et al. (2014), using a combination of potential flow and RANS solvers Paulsen et al. (2014) and focused breaking waves using REEF3D Bihs et al. (2017) are some examples. In all these investigations, the basis of focused wave generation is irregular wave generation. The JONSWAP wave spectrum is used to determine the wave amplitudes and frequencies of individual wave components of the wave train to be generated. In the case of irregular wave generation in numerical wave tanks, a random variable between $[0,2\pi]$ is used to obtain random wave phases. For the generation of focused waves, the wave phases are manipulated in such a way that all wave components propagate a certain distance and concentrate at a given location and time. This implementation for irregular wave generation using the JONSWAP spectrum results in a wave train with large amplitude components around the spectral peak, relatively close to the desired focused wave height. As a result, the generated components are relatively steep for large target focused heights. This introduces two challenges for extreme wave generation using focused waves. The resulting non-linearity due to the high steepness of the components makes

the correct prediction of the focusing point and time difficult Bihs et al. (2017). Further, for larger focused heights, the highly steep components start to break prematurely before they reach the concentration point and the desired focus wave height is not reached.

In the current study, the transient wave packet method Clauss and Kuehnlein (1997) is implemented to simulate large extreme waves and focused breaking waves in the open-source CFD code REEF3D Bihs et al. (2016). The wave packets are optimised using a custom amplitude spectrum, where the high frequency components have been adjusted to avoid premature breaking of these components before the concentration point. Compared to the JONSWAP-based focused waves, the amplitude spectrum used in the study is wider and consists of more harmonic components where each of them is of relatively lower amplitude compared to the target focused height. As a result, larger focused heights can be achieved, while the individual components are less affected by nonlinearity and premature breaking. The implementation is validated using experimental data for a non-breaking focused wave. This model is then used to simulate a breaking focused wave in a two-dimensional numerical wave tank and the wave breaking point is determined. A three-dimensional numerical wave tank is then used to simulate the interaction of a focused breaking wave with a vertical cylinder using the wave characteristics calculated in the two-dimensional wave tank.

2 Numerical Model

The incompressible Unsteady Reynolds-Averaged Navier-Stokes (URANS) equations are used to solve the fluid flow problem in the model REEF3D Bihs et al. (2016):

$$\frac{\partial u_i}{\partial x_i} = 0 \tag{1}$$

$$\frac{\partial u_i}{\partial t} + u_j \frac{\partial u_i}{\partial x_j} = -\frac{1}{\rho}\frac{\partial p}{\partial x_i} + \frac{\partial}{\partial x_j}\left[(\nu + \nu_t)\left(\frac{\partial u_i}{\partial x_j} + \frac{\partial u_j}{\partial x_i}\right)\right] + g_i \tag{2}$$

where the indices i and j=1,2,3 denote the Einstein convention for implicit sum, u is the time averaged velocity, ρ is the density of water, p is the pressure, ν is the kinematic viscosity, ν_t is the eddy viscosity, t is time and g is the acceleration due to gravity. Chorin's projection method Chorin (1968) is used for the pressure treatment and point-wise smoothened fully multi-grid (PFMG) Ashby and Falgout (1996) preconditioned Bi-conjugate gradients stabilised (BiCGStab) solver van der Vorst (1992) is used to solve for the pressure using the high-performance solver library HYPRE Center for Applied Scientific Computing (2006).

The k-ω URANS turbulence model Wilcox (1994) is implemented. To avoid unphysical overproduction of turbulence in strained flow, the eddy viscosity, ν_t, is bounded as shown by Durbin Durbin (2009). In a two-phase model the standard URANS turbulence models do not account for the dissipating effect of the free surface. A free surface turbulence damping algorithm is introduced around the interface based on the studies by Naot and Rodi Naot and Rodi (1982) to avoid the overproduction of turbulence at the free surface due to the large density gradient.

The fifth-order conservative finite difference Weighted Essentially Non-Oscillatory (WENO) scheme proposed by Jiang et al. Jiang and Shu (1996) is used for the discretisation of convective terms for the velocity u_i, and the Hamilton-Jacobi version of the WENO scheme Jiang and Peng (2000) is used for the level set function ϕ, turbulent kinetic energy k and the specific turbulent dissipation rate ω. A Total Variation Diminishing (TVD) third-order Runge-Kutta

explicit time scheme is employed for time discretisation. This scheme is used for the time advancement of the level set function and the reinitialisation equation. Adaptive time stepping is used to maintain optimal time steps throughout the simulation using a fixed Courant number of 0.1, following the validation presented by Bihs et al. Bihs et al. (2016).

A Cartesian grid is used in the numerical model for spatial discretisation. A ghost cell immersed boundary method (IBM) Berthelsen and Faltinsen (2008) is used to incorporate the boundary conditions for complex geometries.The free surface is obtained using the level set method where the zero level set of a signed distance function, $\phi(\vec{x},t)$ is used to represent the interface between air and water. The level set function is reinitialised after every iteration using a partial differential equation (PDE) based reinitialisation procedure presented by Sussman et al. Sussman et al. (1994) to retain its signed distance property after convection. The computational efficiency of the program is increased by using MPI (Message Passing Interface) to run it as a fully parallel code on multiple processors.

Generation of wave packets and active wave absorption

The wave packets generation uses a shape amplitude Fourier spectrum of the form Henning (2005):

$$|F| = \frac{27\left(\omega-\omega_{beg}\right)\left(\omega-\omega_{end}\right)^2}{4\left(\omega_{end}-\omega_{beg}\right)^3} \tag{3}$$

Here, ω is the angular frequency and the subscripts *beg* and *end* confine the Fourier spectrum on the x-axis. The absolute magnitude of the resulting wave amplitude A_i' does not represent the given focused wave input at this point, so a scaling factor f is calculated:

$$f = \frac{A_{focus}}{\sum_{i=1}^{N} A_i'} \tag{4}$$

where A_{focus} is the focused wave amplitude, N is the number of wave components Then the amplitudes of the harmonic components can be calculated as:

$$A_i = fA_i' \tag{5}$$

The free surface, $\eta^{(1)}$ at the wave generation is then calculated as:

$$\eta^{(1)} = \sum_{i=1}^{N} A_i cos\theta_i \tag{6}$$

where, A_i is the amplitude of the each wave component and θ_i is the phase of the each component, which is defined as:

$$\theta_i = k_i x - \omega_i t - \epsilon_i \tag{7}$$

where k_i is the wave number of each component. The parameter ϵ_i is the phase angle, which is chosen in such a way that each wave component focuses at a specified time t_F and location x_F. Second-order irregular wave theory is used as it takes into account wave-wave interaction. The second-order part is added to first-order part for the free surface and the flow velocities. The second-order wave components are implemented using second-order irregular wave theory Schäffer (1996) as formulated by Ning et al. Ning et al. (2009). At the inlet, the free surface and velocities are prescribed through a simple Dirichlet boundary condition. At the downstream end of the tank, waves are absorbed using active wave absorption Schäffer

and Klopman (2000), where a wave opposite to the reflected one is generated by prescribing the following horizontal velocity based on shallow water theory at the downstream boundary:

$$u = \sqrt{\frac{g}{h}}\eta \tag{8}$$

The use of the active wave absorption gives the advantage that an additional part of the domain reserved for wave absorption such as a sponge layer or a relaxation zone is avoided.

3 Results

Validation of wave generation in the numerical wave tank

Experimental wave packet data measured in the Large Wave Flume (GWK), Hannover, Germany Pakozdi (2005) is reproduced in the numerical wave tank to validate the CFD model. The experiments were carried out in a 300 m long channel with a water depth of $d = 4.01$ m. Symmetry conditions are applied on the side walls of the two dimensional wave tank. The wave packets were generated using a Piston-type wavemaker such that the waves concentrate at a distance of $x_f = 126.21$ m from the wavemaker at time $t_f = 103$ s with a focused amplitude of $A_f = 0.75$ m. In order to replicate these results, a 2D numerical wave tank 200 m long with a water depth of $d = 4.01$ m is used with a uniform grid size of $dx = 0.05$ m. The distance of the concentration point from the wavemaker and the time at which it the focused wave is formed is the same as in the experiments, $x_f = 126.21$ m and $t_f = 103$ s respectively. The values for ω_{beg} and ω_{end} are given to be 0.2 and 3.5 Hz respectively, as in the experiments. The number of wave components for the generation of the transient wave packets is chosen to be $N = 500$ based on previous studies on irregular waves. The method of transient wave packets does not seem to be significantly influenced by this, but a detailed study is not carried out. The free surface in the numerical wave tank during wave packet propagation at $t = 76.0$ s and wave focusing at $t_f = 103.0$ s and decomposed wave packets after focusing at $t = 24.0$ s are presented in Figs. (1a), (1b) and (1c) respectively. Turbulent eddies in the air due to the formation of a large wave amplitude after wave focusing are also seen in the Figs. (1b) and (1c).

The free surface elevations measured at several locations in the numerical wave tank are compared to experimental observations and presented in Figs. (2a-2e). At the point of concentration, the focused wave crest elevation in the numerical results is 0.87% higher than the wave crest elevation in the experimental data. The generated waves seen in Fig. (2a) consist of individual waves of different wave heights and frequencies. Figure (2b) shows the propagation of the waves while mostly retaining their form at $x_2 = 50.05$ m. The waves begin to focus as they propagate further to $x_3 = 79.05$ m and $x_4 = 100.10$ m, as seen in Fig. (2c) and Fig. (2d). The wave packet focuses at the prescribed location $x_f = 126.21$ at the prescribed time $x_t = 103.0$ s as seen in Fig. (2e). The numerical results from REEF3D agree well with the experimental data for the wave packet generation, propagation and focussing process throughout the length of the domain. The decomposition of the focused waves after the focusing point at $x = 140.0$ m and $x = 160.0$ m is seen in Figs.(3a) and (3b). The wave elevations presented in Figs. (1c), (3a) and (3b) show that the wave packets propagate towards the focus point, generate an extreme wave at the focus location and then decompose into wave packets as they proceed further in the tank. There are wave reflections in the tank before wave focusing and therefore the choice of the numerical beach does not have any significance on the wave focusing.

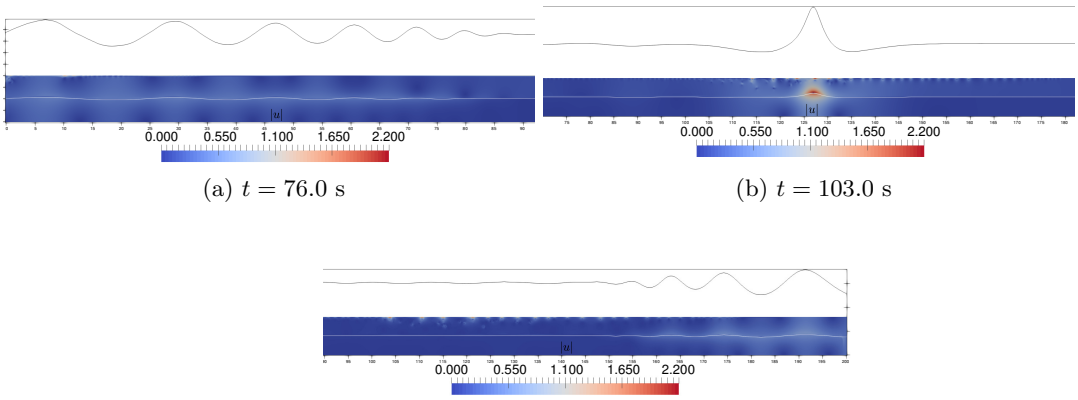

(a) $t = 76.0$ s

(b) $t = 103.0$ s

(c) $t = 120.0$ s

Figure 1: Free surface elevation in the numerical wave tank with velocity magnitude contours and magnified free surface showing the propagation, focussing and defocussing of the wave packets

Replication of wave packet focusing in a shorter numerical domain

The validation of the numerical wave tank for the generation, propagation and focusing of the wave packets is carried out such that the length of the numerical wave tank spans over the distance the wave packets propagated in the experiments before focusing. In order to reduce the computational demand of simulations with focused wave packets, it is prudent to replicate the results in a numerical wave tank of a shorter length. In this section, the length of the numerical wave tank is gradually reduced from 200 m to 25 m to reproduce the same wave as in the previous section. A uniform grid size of $dx = 0.05$ m is used in all the cases. The different lengths of the numerical wave tank, the prescribed time and location for wave focusing is presented in Table 1, along with the difference between the numerical and the expected focused wave crest elevation. The difference in the wave crest height is calculated as $\frac{\eta_{crest,numerical} - \eta_{crest,experimental}}{\eta_{crest,experimental}}$. The difference in the total wave height is calculated in the same way while considering the wave height to be the height from the preceding wave trough level to the focused wave crest level. The results summarised in Table (1), show that the wave

No.	Tank length [m]	x_f [m]	t_f [s]	Difference [%]	
				crest	height
1.	200	126.21	103.0	+0.87	+0.93
2.	100	90.0	60.0	+1.06	−1.31
3.	50	35.0	25.0	+4.7	−2.32
4.	25	15.0	15.0	+9.2	−2.68

Table 1: Simulations carried out to study the effect of reduction in the tank length on the focused wave generation along with the difference between the numerical and experimental results used for validation

crest elevation is seen to be higher than the experimental data by about 0.87% in a 200 m long tank and can increase up to 9.2% higher in a 25 m long tank. On the other hand, it is

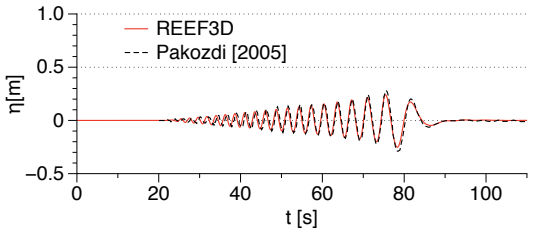

(a) Wave gage close to wave generation at $x_1 = 3.59$ m

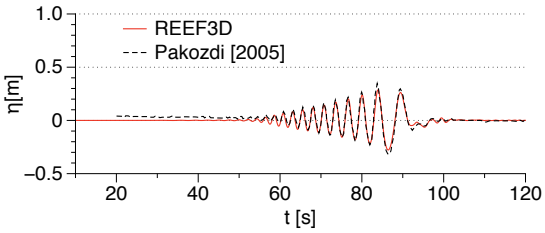

(b) Wave gage at $x_2 = 50.05$ m

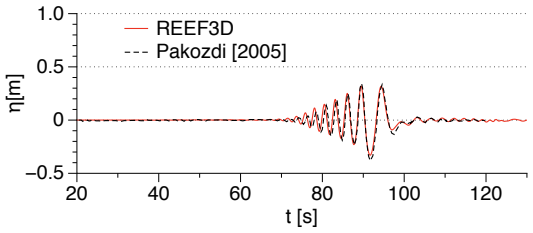

(c) Wave gage at $x_3 = 79.05$ m

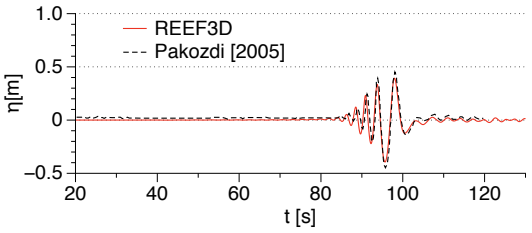

(d) Wave gage at $x_4 = 100.10$ m

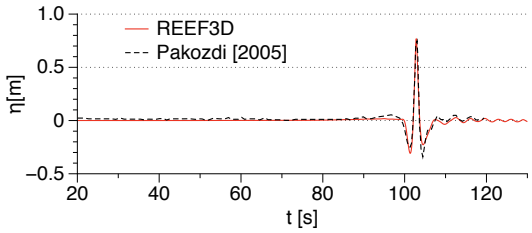

(e) Wave gage at the focus point at $x_f = 126.21$ m

Figure 2: Comparison of the numerical results and experimental data for propagation of wave packets focussing at $x_f = 126.21$ m and $t = 103.0$ s

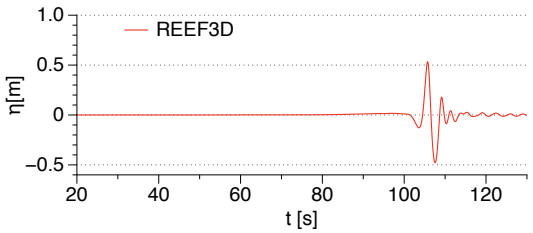

(a) Wave gage at $x_6 = 140.0$ m

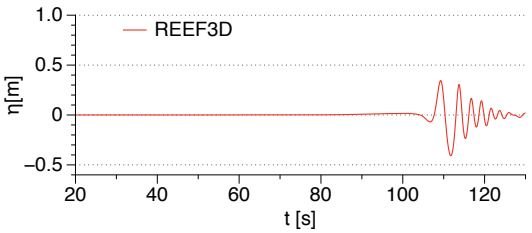

(b) Wave gage at $x_7 = 160.0$ m

Figure 3: Defocusing of the wave packet after passing the focus point at $x_f = 126.21$ s

noticed that the difference in the total wave height is under predicted by only 2.68% for the smallest tank length of 25 m. The discrepancies can be justified as follows. The longer wave tanks provide sufficient distance for the wave packets to propagate and concentrate at the focus point and the results agree well with the experimental data. In the shorter tanks, due

to the smaller distance and shorter time for the propagation of the wave packets, the resulting wave crests are higher than expected, while the troughs are shallower, thus conserving the total wave height. Due to the fact that the wave crest elevations are the most significant contributors to the wave forces on a structure and the differences are less than 10%, this behaviour is considered to be acceptable.

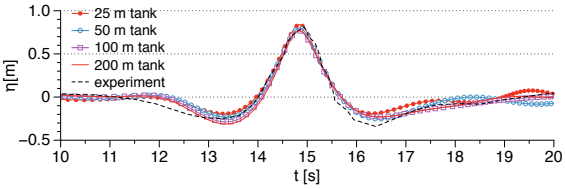

Figure 4: Comparison of free surface elevation at the focus point for all the different tank lengths simulated along with the free surface in the experiments. The results are shifted along the $x-$axis to obtain a comparison of the focused amplitude in the all the cases

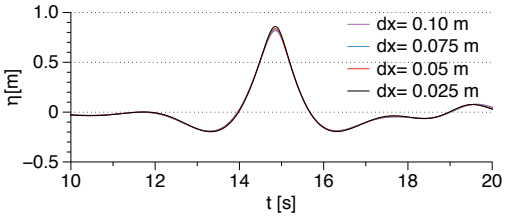

Figure 5: Comparison of free surface elevation at the focus point $x_f = 15.0$ m at time $t_f = 15.0$ s in a 25 m long numerical wave tank

A grid convergence study is carried out for the shorter numerical wave tank with a length of 25m, with focus point $x_f = 15.0$ m and $t_f = 15.0$ s with grid sizes dx= 0.1 m, 0.075 m, 0.05 m and 0.025 m. The comparison of the free surface elevations in the different simulations at the focus point is presented in Fig.(5) and the numerical results at all the grid sizes are seen to be similar. The convergence ratio Stern et al. (2001) for the focused wave crest is calculated using $dx = 0.10$ m, $dx = 0.05$ m and $dx = 0.025$ m as the coarse, medium and fine grids for the analysis. The convergence ratio $R = \epsilon_{mf}/\epsilon_{cm}$, where ϵ_{mf} is the change in the free surface value between the medium and coarse grid, and ϵ_{cm} is the change between the coarse and medium grids. A convergence ratio of $R = 0.90$ is obtained, which implies that the solution is monotonically converging since the $R \in [0, 1]$ indicates monotonic convergence.

Focused wave breaking

In this section, the focus height of the wave packets is increased, so that breaking takes place. Breaking waves simulated in this study correspond to steepness-induced or deep water wave breaking, as the wave train does not undergo shoaling on a reducing water depth in the case as of depth-induced breaking. The phenomenon of steepness-induced breaking is important from the point of view of breaking waves at offshore locations under extreme weather conditions. In this section, the simulations are performed in a wave tank without structures and a two-dimensional setup is sufficient for this case. Focused wave packets are generated in a 25 m long

numerical wave tank with a water depth of $d = 4.01$ m with a focus amplitude of $A_f = 1.35$ m and a uniform grid size $dx = 0.05$ m. The wave breaks at $x_b = 13.70$ m at time $t_b = 13.90$ s with a height of $H_b = 1.75$ m. The breaking wave crest elevation is 1.35 m. Due to the non-linearities involved in waves of large amplitude and wave breaking, the propagating wave crest attains a vertical front slightly earlier than the prescribed focus time of $t_f = 15.0$ s and at a location earlier than the focus distance of $x_f = 15.0$ m. The individual wave components are not subject to breaking, but they focus earlier than the theoretical prediction and the focused wave then breaks. A grid convergence study is carried out for the breaking focused wave using grid sizes $dx = 0.10$ m, $dx = 0.075$ m, $dx = 0.05$ m and $dx = 0.03$ m and presented in Fig. (6). It is seen that the vertical breaking wave profile is achieved at $x_b = 13.70$ m for $dx = 0.05$ m and $dx = 0.03$ m. Thus, $dx = 0.05$ m is considered to be sufficient to represent the breaking wave kinematics. The evolution of the breaking wave is shown in Fig. (7).

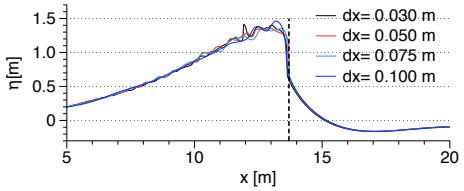

Figure 6: Grid convergence study for the breaking wave with focused amplitude $A_f = 1.35$ m, with the vertical front marked at the breaking location $x_b = 13.70$ m

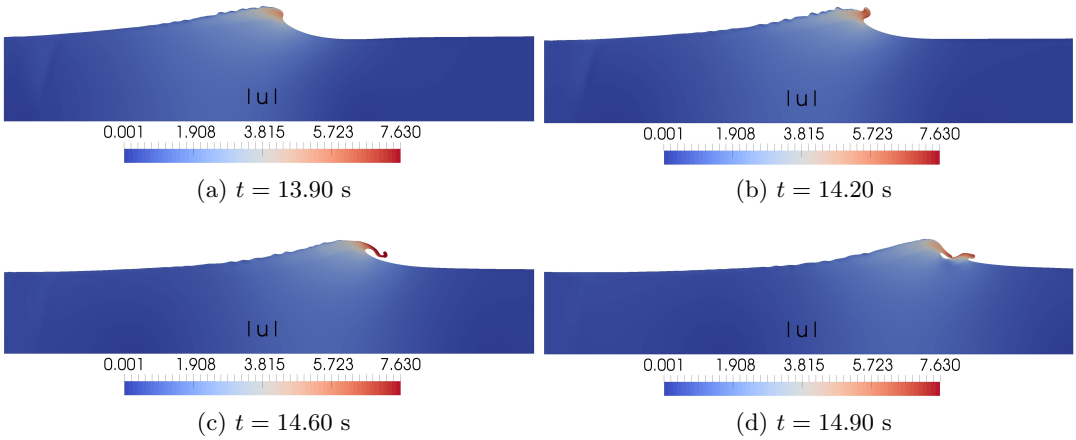

(a) $t = 13.90$ s (b) $t = 14.20$ s

(c) $t = 14.60$ s (d) $t = 14.90$ s

Figure 7: Evolution of the breaking wave produced by focussing wave packets with a target focus amplitude $A_f = 1.35$ m in a water depth of $d = 4.01$ m

Breaking wave forces due to focused wave breaking

The focused breaking wave packet presented in the previous section is simulated in a three-dimensional numerical wave tank of length 25 m and width 5 m with a water depth $d = 4.01$ m. As in the 2D case, a uniform grid size $dx = 0.05$ m and a fixed Courant number of

0.1 for the adaptive time stepping is used. No-slip wall conditions are applied on the side walls and the bottom of the tank. No-slip conditions are also employed on the surface of the obstacle. A vertical cylinder with diameter $D = 0.7$ m is placed at $x = 15.0$ m. The cylinder corresponds to a $1 : 8.6$ scale of an offshore wind substructure at the alpha ventus test site Wienke and Oumeraci (2005). The wave breaking point is determined to be $x_b = 13.2$ m and the overturning wave crest impacts the surface of the cylinder just below the wave crest level at $x = 14.65$ m. This location of the cylinder with respect to the wave breaking point results in large breaking wave forces Irschik et al. (2002); Kamath et al. (2016). The calculated wave forces on the cylinder are presented in Fig.(8). The impulsive nature of breaking wave forces is seen in Fig.(8) with a sharp peak in the plot for wave force over time. The peak force occurs just after $t = 14.1$ s with a peak force of 17150 N. This value is comparable to the total wave force of 12350 N calculated on the same cylinder placed on a $1 : 10$ slope due to a breaking wave height $H_b = 1.30$ m under a similar wave impact scenario Choi et al. (2015) Kamath et al. (2016). While the previous studies present depth induced wave breaking, the current study presents the interaction of steepness induced breaking waves in deep water. The evolution of the breaking wave and its interaction with the cylinder is presented in Figs.(9a and 9b). The breaking wave impacts the cylinder at $t = 14.1$ s in Fig.(9a). The broken wave separating around the cylinder after impact is shown in Fig.(9b).

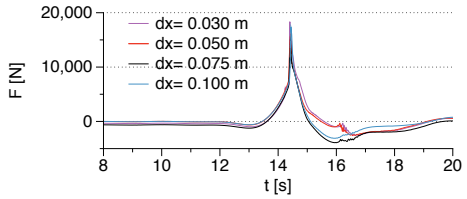

Figure 8: Grid convergence for the wave forces due to the focused breaking wave of amplitude $A_f = 1.35$ m

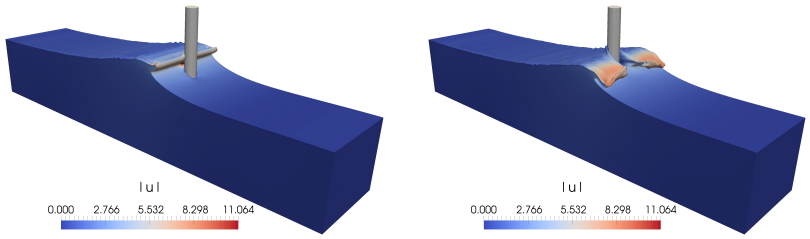

(a) $t = 14.1$ s (b) $t = 14.4$ s

Figure 9: Interaction of the overturning wave crest with a vertical cylinder

The pressure distribution over the depth in front and behind the cylinder during different stages of the focused breaking wave impact on the cylinder are presented in Fig.(10). The hydrostatic pressure (p_{hs}) due to the still water level is subtracted from the total pressure (p) to obtain the dynamic pressure presented in Fig.(10). The pressure distribution is seen to be almost hydrostatic just before the overturning wave crest impacts the cylinder at $t = 13.9$ s

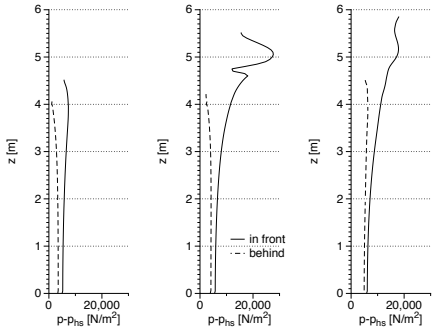

(a) $t = 13.9$ s (b) $t = 14.3$ s (c) $t = 14.6$ s

Figure 10: Dynamic pressure in front and behind the cylinder during the impact of the focused breaking wave

in Fig.(10a). The large difference in pressure in front and behind the cylinder that results in the large impact forces during the interaction of the focused breaking wave with the cylinder at $t = 14.3$ s is presented in Fig.(10b). The difference in the pressure in front and behind the cylinder is reduced once the overturning wave crest has passed the cylinder at $t = 14.6$ s in Fig.(10c).

4 Conclusions

The method of a customised amplitude spectrum to generate focused waves using the transient wave packets method Clauss and Kuehnlein (1997) has been implemented in the open-source CFD model REEF3D. The implementation is validated by comparing the numerical results with experimental results from the Large Wave Flume (GWK), Hannover, Germany for a non-breaking focused wave. Then, simulations are carried out to replicate the focused wave after propagation of the wave packets over a shorter distance and for a shorter time compared to the validation case, in order to reduce the computational demand for such simulations. Further, simulations for steepness-induced deep water wave breaking using focused wave packets are carried out. The breaking point and the wave breaking height are determined in two-dimensional simulations. Finally, a three-dimensional simulation is carried out to demonstrate the calculation of total breaking wave forces on a vertical cylinder. The study demonstrates a numerical model to evaluate extreme wave forces on an offshore structure with the representation of a continuously changing envelope of an extreme wave train. The following conclusions can be drawn from the study:

1. The transient wave packet method to generate focused breaking waves is presented. The numerical model is able to represent the transient wave packet propagation and focussing well and the numerical results agree well with the experimental observations.

2. The length of the NWT is reduced compared to the experiments to obtain wave focusing using this method in a much smaller domain. It is seen that the model is able to reproduce the wave with a 9% higher wave height after reducing the travel distance for focus by 8.3 times compared to the original full-sized tank. Given that the difference in the total wave height is not significant and that the wave crest which determines the maximum wave forces is not under estimated, this is considered acceptable.

3. The method is then used to produce a steepness induced breaking wave (deep water breaking wave) by setting a target focused wave height at the limit of wave breaking in the reduced length NWT. The model is able to produce such a wave without breakdown of the individual wave components before the focused wave is formed.

4. For the generated wave in the current study, the wave breaking point is 7.3% before and 8.6% behind the theoretical target focus time and location of a non-breaking steep wave. The breaking wave crest height is seen to the same as the target focused wave amplitude.

5. The total breaking wave forces on a cylinder are evaluated after determining the breaking point in a 2D simulation.

Further studies can be carried out to quantify the change in time and location of the breaking point in the simulations in comparison to the theoretically expected focusing location for non-breaking waves. Detailed analysis of the breaking wave physics can also be conducted.

Acknowledgments

This research was supported in part with computational resources at NTNU provided by The Norwegian Metacenter for Computational Sciences (NOTUR, http://www.notur.no), Project No. NN2620K.

References

Ashby, S.F. and Falgout, R.D. (1996). A parallel mulitgrid preconditioned conjugate gradient algorithm for groundwater flow simulations. *Nuclear Science and Engineering*, **124**(1), 145–159.

Berthelsen, P.A. and Faltinsen, O.M. (2008). A local directional ghost cell approach for incompressible viscous flow problems with irregular boundaries. *Journal of Computational Physics*, **227**, 4354–4397.

Bihs, H., Alagan Chella, M., Kamath, A. and Arntsen, Ø.A. (2017). Numerical investigation of focused waves and their interaction with a vertical cylinder using REEF3D. *Journal of Offshore Mechanics and Arctic Engineering*, **139**(4), 041101–1–8.

Bihs, H., Kamath, A., Alagan Chella, M., Aggarwal, A. and Arntsen, Ø.A. (2016). A new level set numerical wave tank with improved density interpolation for complex wave hydrodynamics. *Computers & Fluids*, **140**, 191–208.

Center for Applied Scientific Computing (2006). *HYPRE high performance preconditioners - User's Manual*. Lawrence Livermore National Laboratory.

Chen, L.F., Zang, J., Hillis, A.J., Morgan, G.C.J. and Plummer, A.R. (2014). Numerical investigation of wave–structure interaction using OpenFOAM. *Ocean Engineering*, **88**, 91–109.

Choi, S.J., Lee, K.H. and Gudmestad, O.T. (2015). The effect of dynamic amplification due to a structure's vibration on breaking wave impact. *Ocean Engineering*, **96**, 8–20.

Chorin, A. (1968). Numerical solution of the Navier-Stokes equations. *Mathematics of Computation*, **22**, 745–762.

Clauss, G.F. and Bergmann, J. (1986). Gaussian wave packets -A new approach to seakeeping tests of ocean structures. *Applied Ocean Research*, **8**(4), 190 – 206.

Clauss, G.F. and Kuehnlein, W.L. (1997). A new tool for seakeeping test - nonlinear transient wave packets. In: *8th International Conference on the Behaviour of Offshore Structures, Delft, The Netherlands*.

Durbin, P.A. (2009). Limiters and wall treatments in applied turbulence modeling. *Fluid Dynamics Research*, **41**, 1–18.

Hansen, P.F. and Nielsen, L.P. (1995). On the new wave model for the kinematics of large ocean waves. In: *Proceedings of the International Conference on Offshore Mechanics and Arctic Engineering, Copenhagen, Denmark*.

Henning, J. (2005). *Generation and Analysis of Harsh Wave Environments*. Ph.D. thesis, Technical University Berlin.

Irschik, K., Sparboom, U. and Oumeraci, H. (2002). Breaking wave characteristics for the loading of a slender pile. In: *Proc. 28th International Conference on Coastal Engineering, Cardiff, Wales*.

Jiang, G.S. and Peng, D. (2000). Weighted ENO schemes for Hamilton-Jacobi equations. *SIAM Journal on Scientific Computing*, **21**, 2126–2143.

Jiang, G.S. and Shu, C.W. (1996). Efficient implementation of weighted ENO schemes. *Journal of Computational Physics*, **126**, 202–228.

Kamath, A., Alagan Chella, M., Bihs, H. and Arntsen, Ø.A. (2016). Breaking wave interaction with a vertical cylinder and the effect of breaker location. *Ocean Engineering*, **128**, 105–115.

Naot, D. and Rodi, W. (1982). Calculation of secondary currents in channel flow. *Journal of the Hydraulic Division, ASCE*, **108**(8), 948–968.

Ning, D.Z., Zang, J., Liu, S.X., Taylor, R.E., Teng, B. and Taylor, P.H. (2009). Free-surface evolution and wave kinematics for nonlinear uni-directional focused wave groups. *Ocean Engineering*, **36**, 1226—1243.

Pakozdi, C. (2005). Numerische Simulation nichtlinearer transienter Wellengruppen. Technical report, Technical University Berlin.

Pastoor, W., Helmers, J.B. and Bitner-Gregersen, E. (2003). Time simulation of ocean going structures in extreme waves. In: *Proceedings of the 22nd International Conference on Offshore Mechanics and Arctic Engineering*.

Paulsen, B.T., Bredmose, H. and Bingham, H.B. (2014). An efficient domain decomposition strategy for wave loads on surface piercing circular cylinders. *Coastal Engineering*, **86**, 57–76.

Phillips, O.M., Gu, D. and Donelan, M. (1993). Expected structure of extreme waves in a gaussian sea. part I: Theory and SWADE buoy measurements. *Journal of Physical Oceanography*, **23**(5), 992–1000.

Rozario, J.B., Tromans, P.S., Taylor, P.H. and Efthymiou, M. (1993). Comparison of loads predicted using 'NewWave' and other wave models with measurements on the tern structure. In: *Wave kinematics and environmental forces*, 143–159. Springer.

Schäffer, H.A. (1996). Second-order wavemaker theory for irregular waves. *Ocean Engineering*, **23**(1), 47–88.

Schäffer, H.A. and Klopman, G. (2000). Review of multidirectional active wave absorption methods. *Journal of Waterway, Port, Coastal, and Ocean Engineering*, **126**(2), 88–97.

Soares, C.G. (1993). Long term distribution of non-linear wave induced vertical bending moments. *Marine Structures*, **6**(5-6), 475–483.

Stern, F., Wilson, R.V., Coleman, H.W. and Paterson, E.G. (2001). Comprehensive approach to verification and validation of cfd simulations-part 1: methodology and procedures. *Transactions of the American Society of Mechanical Engineers - Journal of Fluids Engineering*, **123**(4), 793–802.

Sussman, M., Smereka, P. and Osher, S. (1994). A level set approach for computing solutions to incompressible two-phase flow. *Journal of Computational Physics*, **114**, 146–159.

Torhaug, R. (1996). *Extreme response of nonlinear ocean structures: Identification of minimal stochastic wave input for time-domain simulation.* Ph.D. thesis, Stanford University.

Tromans, P.S., Anaturk, A.R. and Hagemeijer, P. (1991). A new model for the kinematics of large ocean waves-application as a design wave. In: *The First International Offshore and Polar Engineering Conference*. International Society of Offshore and Polar Engineers.

van der Vorst, H. (1992). BiCGStab: A fast and smoothly converging variant of Bi-CG for the solution of nonsymmetric linear systems. *SIAM Journal on Scientific and Statistical Computing*, **13**, 631–644.

Wang, L.H. (2001). *Probabilistic analysis of nonlinear wave-induced loads on ships.* Ph.D. thesis, Norwegian University of Science and Technology.

Wheeler, J.D. (1969). Method for calculating forces produced by irregular waves. In: *Proc., Offshore Technology Conference, Dallas.*

Wienke, J. and Oumeraci, H. (2005). Breaking wave impact force on a vertical and inclined slender pile – theoretical and large-scale model investigations. *Coastal Engineering*, **52**, 435–462.

Wilcox, D.C. (1994). *Turbulence modeling for CFD.* DCW Industries Inc., La Canada, California.